ADVANCED FUNCTIONAL MATERIALS
www.afm-journal.de

www.MaterialsViews.com

Size-Controlled Synthesis of $Cu_{2-x}E$ (E = S, Se) Nanocrystals with Strong Tunable Near-Infrared Localized Surface Plasmon Resonance and High Conductivity in Thin Films

*Xin Liu, Xianliang Wang, Bin Zhou, Wing-Cheung Law, Alexander N. Cartwright, and Mark T. Swihart**

A facile method for preparing highly self-doped $Cu_{2-x}E$ (E = S, Se) nanocrystals (NCs) with controlled size in the range of 2.8–13.5 nm and 7.2–16.5 nm, for $Cu_{2-x}S$ and $Cu_{2-x}Se$, respectively, is demonstrated. Strong near-infrared localized surface plasmon resonance absorption is observed in the NCs, indicating that the as-prepared particles are heavily p-doped. The NIR plasmonic absorption is tuned by varying the amount of oleic acid used in synthesis. This effect is attributed to a reduction in the number of free carriers through surface interaction of the deprotonated carboxyl functional group of oleic acid with the NCs. This approach provides a new pathway to control both the size and the cationic deficiency of $Cu_{2-x}Se$ and $Cu_{2-x}S$ NCs. The high electrical conductivity exhibited by these NPs in metal-semiconductor-metal thin film devices shows promise for applications in printable field-effect transistors and microelectronic devices.

1. Introduction

Semiconductor nanocrystals are of interest due to their tunable size- and shape-dependent physical and chemical properties.[1,2] These materials, which are commonly synthesized by wet chemical methods,[3,4] have enormous potential for application in future low-cost solution-processed photovoltaic,[5–12] microelectronic,[13–16] and optoelectronic devices.[17–19] Copper-based chalcogenide nanocrystals[20–31] and related alloys[32–42] have attracted much interest due to their lack of toxicity, low cost, and ability to achieve band-gap energies of 1.0–1.5 eV, which are well matched to the solar spectrum at the earth's surface. In 2009, Zhao et al.[43] proposed that NIR absorbance observed in cation-deficient $Cu_{2-x}S$ NCs originates from localized surface plasmon resonance (LSPR) of free holes in the valence band. This contrasts with the previous interpretation of this absorbance as arising from an indirect band gap. In 2011, Luther et al.[44] presented a combined experimental and theoretical study that conclusively demonstrated that this absorbance is due to plasmon resonance of free holes in $Cu_{2-x}S$ nanocrystals. Meanwhile, Dorfs et al.[45] studied the blue-shift of optical absorbance of $Cu_{2-x}Se$ nanocrystals upon gradual, controlled oxidation, which increased the concentration of cation vacancies. These and other recent investigations[46] not only extend studies of LSPR from well-known metals to heavily-doped semiconductor NCs but may also provide a new pathway for utilizing and controlling NIR optical energy.[47–49]

While many previous reports have studied synthesis and optical properties of copper chalcogenide NCs,[9,20–26,50–54] few have demonstrated the existence of NIR absorbance. Stoichiometric Cu_2S and Cu_2Se NCs or slightly cation-deficient $Cu_{2-x}S$ and $Cu_{2-x}Se$ with low values of x do not have sufficient free carriers to exhibit LSPR. Alivisatos and co-workers[44] synthesized 3–6 nm diameter monodisperse $Cu_{2-x}S$ NCs and demonstrated, by a combination of experimental and theoretical studies, that their NIR absorbance originated from a localized surface plasmon resonance of the free holes in the NCs. The LSPR peak in that study was located around 0.7 eV, indicating a relatively low free carrier concentration. Manna and co-workers[45] did pioneering work in the synthesis of $Cu_{2-x}Se$ NCs with clear NIR plasmonic absorbance. However, byproducts, including large NCs with a different crystal structure, were also formed. We are not aware of any previous reports of size-tunable synthesis of monodisperse $Cu_{2-x}Se$ NCs with significant LSPR. Here we demonstrate such a method, applicable to both $Cu_{2-x}Se$ and $Cu_{2-x}S$. By adjusting reaction conditions, we achieve different sizes and crystal structures. Moreover, we are able to tune the NIR LSPR wavelength by simply adjusting the reaction conditions without applying a separate controlled oxidation process.

X. Liu, X. Wang, Prof. M. T. Swihart
Department of Chemical and Biological Engineering
University at Buffalo (SUNY)
Buffalo, NY 14260. USA
E-mail: swihart@buffalo.edu
B. Zhou, Prof. A. N. Cartwright
Department of Electrical Engineering
University at Buffalo (SUNY)
Buffalo, NY 14260. USA
Dr. W.-C. Law
Institute for Lasers
Photonics, and Biophotonics
University at Buffalo (SUNY)
Buffalo, NY 14260. USA

DOI: 10.1002/adfm.201202061

2. Synthesis of $Cu_{2-x}Se$ NCs with Tunable Size and Crystal Structure

We began this study using the well-established approach based upon preparing the organo-selenium precursor by dissolving selenium powder in alkyl-phosphines. However, colloidal $Cu_{2-x}Se$ NCs synthesized by injecting trioctylphosine (TOP) or tributylphosphine (TBP) selenium solutions into hot solutions of copper precursors were generally polydisperse and colloidally unstable, and did not exhibit strong LSPR absorbance. Because of the relatively strong reducing ability of the alkyl phosphines, synthesis using them tends to produce either stoichiometric Cu_2Se NCs without the cation deficiency required to produce LSPR, or $Cu_{2-x}Se$ with a small value of x and broad, weak LSPR absorbance.[24]

Because part of our goal was to generate copper vacancies and strong LSPR absorbance in the NCs, we studied other methods of preparing organo-selenium precursors. Oleylamine (OAm) and oleic acid (OA) are extensively used to stabilize colloidal nanocrystals. We have used each of these two ligands to dissolve selenium powder, forming OAm-Se and OA-Se organo-selenium donors, respectively. Our general reaction model is based on dissolving Cu(I)Cl powder in OAm or OAm/OA mixtures, then injecting the selenium precursor into the hot copper precursor solution. Monodisperse $Cu_{2-x}Se$ NCs with tunable size, shape, and crystal structure can be achieved by adjusting the reaction conditions. Additionally, this phosphine-free method does not require handling reagents under oxygen-free conditions, as would be required when using alkyl-phosphines. Finally, the precursors used in this method are low cost and commercially available in large quantities.

2.1. Oleylamine-Based Synthesis of $Cu_{2-x}Se$ NCs

Synthesis of $Cu_{2-x}Se$ NCs in pure oleylamine was performed by injecting Se-OAm complexes into Cu-OAm solution at 210–220 °C. TEM imaging of particles extracted and quenched within the first five minutes after injection (**Figure 1**a-f) showed that the particles were quite monodisperse. Powder X-ray diffraction

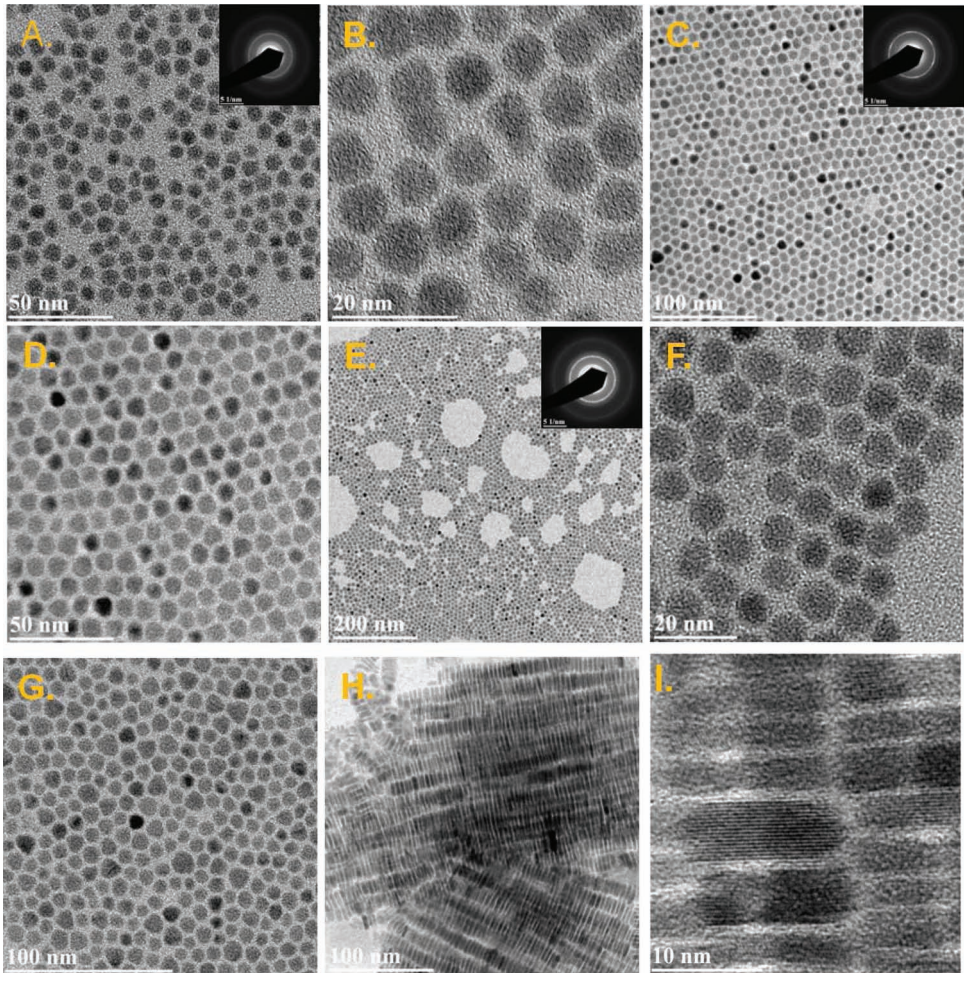

Figure 1. TEM images showing time-dependent size evolution of $Cu_{2-x}Se$ NCs: A,B) 7.2 ± 0.9 nm $Cu_{2-x}Se$ NCs at 1.5 min reaction time; C,D) 8 ± 0.8 nm $Cu_{2-x}Se$ NCs at 3 min reaction time; E,F) 9.2 ± 1.2 nm $Cu_{2-x}Se$ NCs at 5 min reaction time; G) Classic Ostwald ripening at 8.5 min; and H,I) $Cu_{2-x}Se$ nanodisks. Size distributions obtained by counting 100 particles of each sample are available in the Supporting Information.

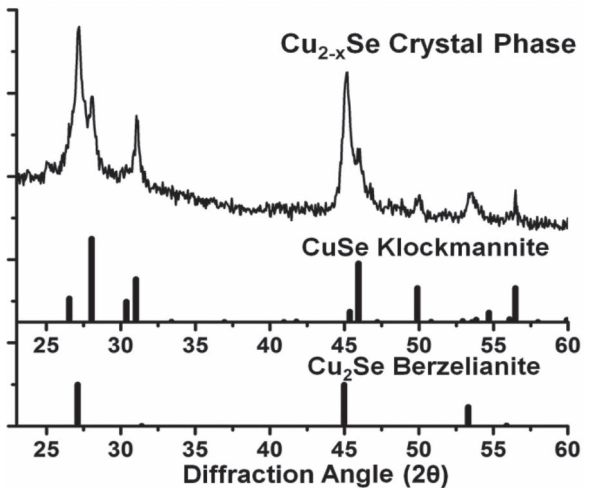

Figure 2. Powder XRD pattern from $Cu_{2-x}Se$ NCs at 5 min reaction time, showing that they are a mix of klockmannite (CuSe, PDF Card 03-065-3562) and berzelianite (Cu_2Se, PDF card 01-088-2043) phases.

(XRD, **Figure 2**) showed that the product particles were a mixture of CuSe (klockmannite) and Cu_2Se (berzelianite) phases at all reaction times. For particles produced at 5 min reaction time, we estimated the phase fractions of klockmannite and berzelianite to be 35.7% and 64.3%, respectively, based upon Reitveld refinement fitting of the XRD pattern shown in Figure 2. The resulting fit, obtained using the MAUD program,[55] is shown in Supporting Information Figure S5. The monodisperse growth of $Cu_{2-x}Se$ NCs is attributed to the size-focusing effect as embodied by Equation 1, where V' is the rate of volume growth of a nanocrystal, d is the diameter and d' is the linear growth rate. In the initial stages of reaction, following a burst of nucleation, particle growth is limited by diffusion of monomers to nuclei, resulting in a constant volumetric growth rate. Under these conditions, smaller particles have higher linear growth rate than larger particles and therefore tend to "catch up" with larger particles and narrow the size distribution.

$$V' = \frac{\pi}{2}\left(d^2\right)d' = \text{constant} \quad (1)$$

It is worth mentioning that the impurity profile of OAm can influence the morphology of $Cu_{2-x}Se$ NCs. By investigating OAm from Sigma Aldrich (technical grade 70%, and >98% primary amine) and Fisher Scientific (80–90% C18 compounds, 97% primary amine), we found that OAm from Sigma Aldrich consistently produced quasi-spherical $Cu_{2-x}Se$ NCs (Figure 1A–G), while nanodisks were always observed when OAm from Fisher Scientific was used. While we have not investigated the origin of this difference in detail, the change in morphology upon changing the source of the oleylamine was reproducible. We report it here to emphasize the potential sensitivity of the nanocrystal morphology to the composition of the coordinating solvent.

2.2. The Effect of Oleic Acid on $Cu_{2-x}Se$ Nanocrystal Growth

To study the influence of oleic acid on $Cu_{2-x}Se$ nucleation and growth, we first varied the concentration of OA in the Cu(I) precursor solution while using only OAm in the Se precursor solution. The particle size increased with increasing OA concentration, and the resulting nanocrystals were rather polydisperse (Supporting Information Figure S6). This implies that the introduction of oleic acid accelerates the decomposition of the precursors, forming nuclei with a broad size distribution. The Ostwald ripening stage of growth then occurred earlier, due to faster depletion of monomers compared to the pure OAm system. The observed polydispersity, along with the difficulty of dissolving CuCl in pure OA led us to explore addition of OA to the Se precursor solution instead.

To the best of our knowledge, this is the first demonstration of the use of Se-OA and S-OA precursors prepared by simply dissolving selenium or sulfur powder in pure OA. This general approach provides a new phosphine-free route for preparing semiconductor nanocrystals. Similar to the observation of Hanrath and co-workers,[56] oleic acid was observed to reduce the rate of particle growth by reducing the reactivity of the selenium donor (Se-OA complex). Use of the Se-OA precursor in 1) pure OAm, 2) a 2:1 OAm/OA mixture, or 3) a 1:2 OAm/OA mixture produced nearly mono-disperse 5 nm, 8 nm or 16 nm $Cu_{2-x}Se$ NCs, respectively. **Figure 3** presents TEM images of these particles of varying size. Although the reaction time for these syntheses extended beyond 5 min, the size distribution remained quite narrow. This supports the hypothesis that the use of OA-bound chalcogenide donors reduces the rate of monomer depletion, extending the size-focusing growth regime to longer reaction time. Powder XRD (**Figure 4**) showed that these particles had the berzelianite crystal structure. In contrast to $Cu_{2-x}Se$ NCs synthesized using only OAm, no diffraction peaks attributable to klockmannite CuSe were present.

2.3. Size-Tunable $Cu_{2-x}S$ NCs

Building upon our general reaction model for synthesizing $Cu_{2-x}Se$ NCs, we prepared copper sulfide NCs by an analogous approach. **Figure 5**A–F shows $Cu_{2-x}S$ NCs with tunable average sizes ranging from 2.8 nm to 13.5 nm. These monodisperse $Cu_{2-x}S$ NCs were reproducibly prepared with control of their size by varying reaction conditions such as activation temperature, aging temperature, and reaction time (see Experimental Section for details). Figure 5E,F show images of mono-disperse $Cu_{2-x}S$ nanocrystals synthesized by injecting OA-S complexes into Cu(I)-OAm/OA. Powder XRD patterns (**Figure 6**), which were consistent with the SAED patterns observed in TEM, indicated two major crystal structures: covellite and djurleite, respectively. $Cu_{2-x}S$ NCs synthesized using OA had the covellite crystal structure ($x = 1$). In contrast, $Cu_{2-x}S$ NCs prepared using purely OAm had the djurleite structure and a smaller value of x. Thus, addition of oleic acid during synthesis of $Cu_{2-x}S$ NCs induces oxidation of copper to produce CuS ($x = 1$), in contrast to the results for synthesis of $Cu_{2-x}Se$ NCs, where $x < 1$ was observed for all OA/OAm combinations. While the conventional size-focusing mechanism of diffusion-limited growth (Equation 1) could explain the formation of monodisperse $Cu_{2-x}Se$ NCs described above, this mechanism does not appear to apply to the growth of monodisperse $Cu_{2-x}S$ NCs presented here. Thermogravimetric analysis of $Cu_{2-x}S$ particles from a reaction that

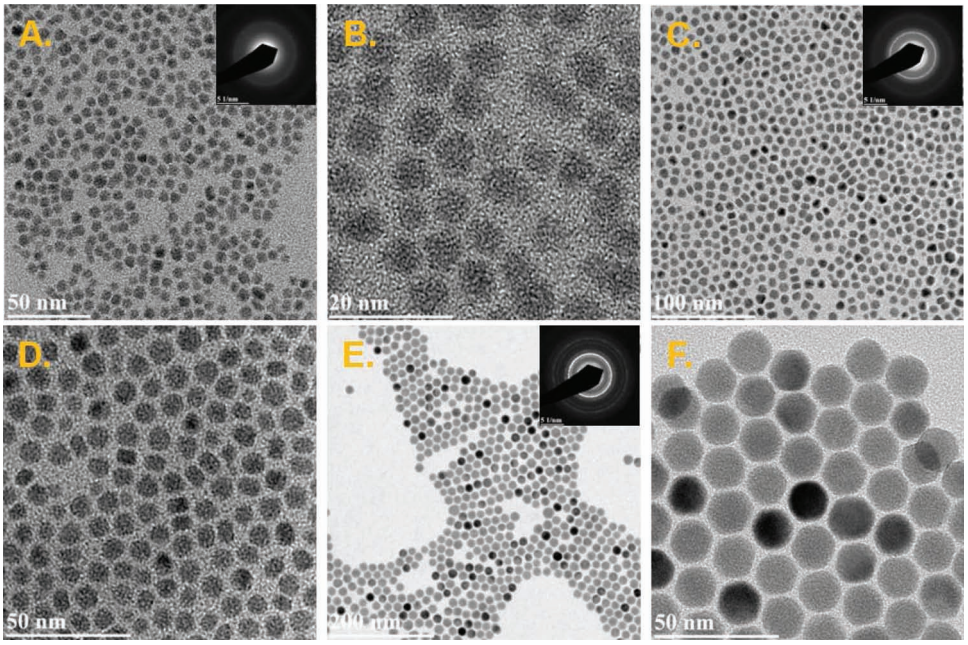

Figure 3. TEM image of $Cu_{2-x}Se$ NCs size evolution with increasing concentration of OA. A,B) 6.2 ± 0.7 nm $Cu_{2-x}Se$ NCs prepared using Cu(I) in pure OAm; C,D) 8.2 ± 1.5 nm $Cu_{2-x}Se$ NCs prepared using Cu(I) in a 2:1 OAm/OA mixture; and E,F) 16.5 ± 1.5 nm $Cu_{2-x}Se$ NCs prepared using Cu(I) in a 1:2 OAm/OA mixture.

was quenched 2 min after injection showed that ≈90% of the monomers had been converted to nanocrystals (**Figure 7**). This does not leave enough monomer remaining in solution to support the observed particle growth from 2 to 5 min. Nonetheless, the particle size distribution remained quite monodisperse as the NCs continued to grow. The maintenance of size-distribution monodispersity can thus most likely be attributed to self-focusing by interparticle diffusion, as proposed by Thessing et al.[57] We estimated an average distance of around 120 nm between individual particles after 2 min of reaction time (Supporting Information). If the particle diffusion sphere radius is more than 60 nm, then this interparticle diffusion phenomenon can be expected to occur.

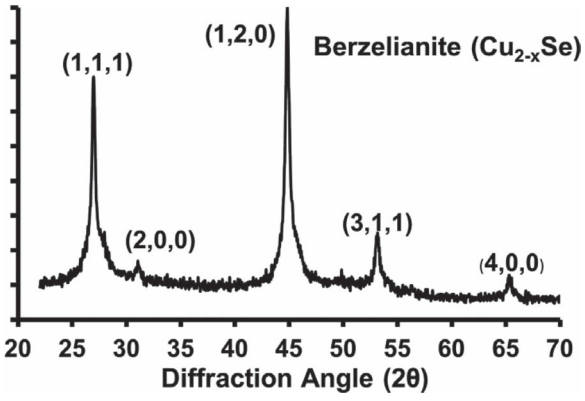

Figure 4. Powder XRD pattern from particles prepared by injecting Se-OA precursor into hot copper-OAm/OA solution, showing only the berzelianite crystal structure.

3. Tunable Localized Surface Plasmon Resonance (LSPR) in $Cu_{2-x}Se$ and $Cu_{2-x}S$ NCs

Recently, Dorfs et al. demonstrated that the LSPR frequency could be tuned by controllably oxidizing $Cu_{2-x}Se$ NCs using $NH_4Ce(NO_3)_6$, to change the charge carrier density in the particles. Kriegel et al.[58] extended this method to $Cu_{2-x}Te$ NCs and studied photoluminescence quenching induced by LSPR. Here we demonstrate a simple alternative method to tune LSPR through in situ control of carrier density in $Cu_{2-x}S$ and $Cu_{2-x}Se$ NCs during synthesis, without the requirement of controlled chemical post-treatment.

To demonstrate the LSPR behavior of the $Cu_{2-x}S$ NCs prepared here, we first investigated the dependence of their NIR absorbance upon the refractive index of the solvents in which they were dispersed. **Figure 8**A and Figure S7 (Supporting Information) show that the NIR absorbance of $Cu_{2-x}S$ NCs red-shifts with increasing refractive index of the surrounding media, as expected for LSPR absorbance. Interestingly, we also observed LSPR frequency shifts when oleic acid, rather than oleylamine alone, was used in the synthesis. The NIR LSPR absorbance red-shifts with increasing amount of oleic acid used in the synthesis, by up to 270 nm in $Cu_{2-x}Se$ NCs (Figure 8B) and by up to 110 nm in $Cu_{2-x}S$ NCs (Figure 8C). Although the LSPR frequency depends somewhat on NC size, the notable red-shift observed here could not be explained by the slight variation in particle size with addition of OA. Figure 8D illustrates schematically a proposed mechanism that may underlie the observed red-shift of LSPR upon addition of oleic acid in the synthesis. Oleylamine coordinates to the surface via its amino functional group, while oleic acid coordinates through the surface via its deprotonated carboxyl functional group, as confirmed by FTIR spectroscopy

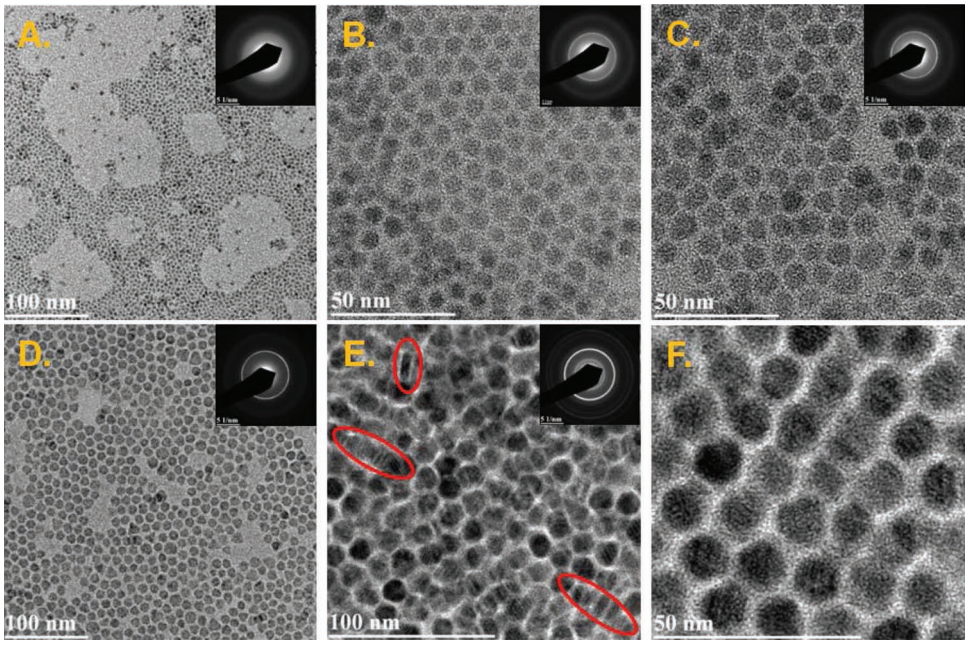

Figure 5. TEM images of $Cu_{2-x}S$ NCs with diverse size and morphology: A) 2.8 ± 0.8 nm $Cu_{2-x}S$ NCs; B) 6.8 ± 0.8 nm $Cu_{2-x}S$ NCs; C) 8.8 ± 1.2 nm $Cu_{2-x}S$ NCs; D) 11.5 ± 1.4 nm $Cu_{2-x}S$ NCs; and E,F) 13.5 ± 1.5 nm $Cu_{2-x}S$.

(see Supporting Information Figure S9). The plasmon resonance requires the presence of a large number of free carriers, which in $Cu_{2-x}Se$ and $Cu_{2-x}S$ NCs are the free holes that are present due to copper deficiency. The uncharged oleylamine ligands are not expected to significantly influence the concentration of free carriers, which is set by the stoichiometry and crystal structure

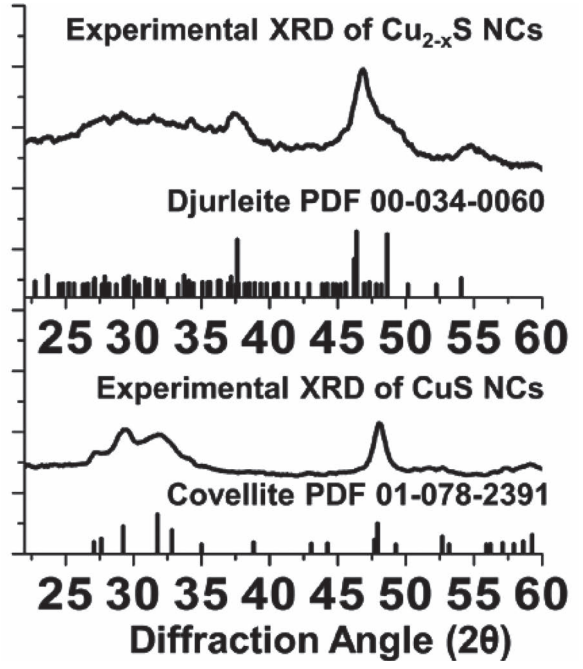

Figure 6. Powder XRD patterns from nanoparticles produced using OA/OAm mixture (top curve) or pure OAm (bottom curve).

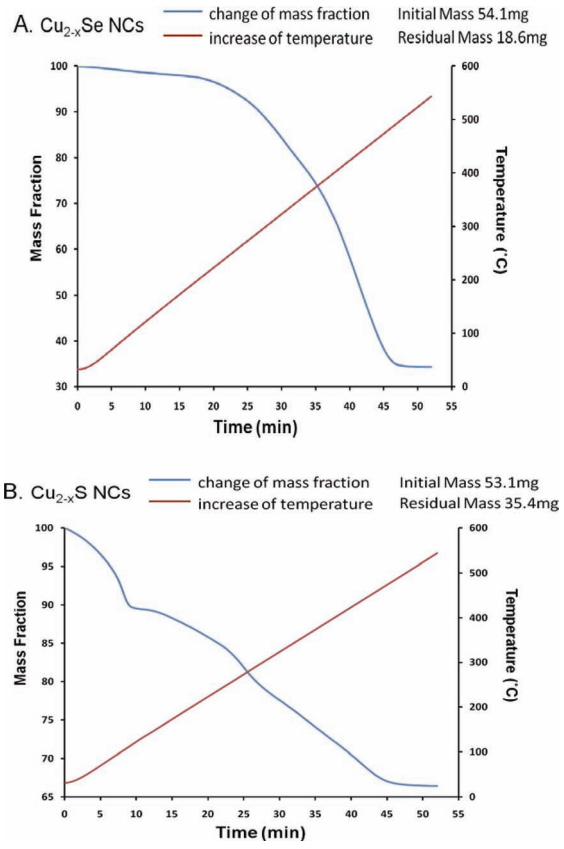

Figure 7. Thermogravimetric analysis of A) entire batch of $Cu_{2-x}Se$ produced after 1.5 min reaction time and B) entire batch of $Cu_{2-x}S$ NCs produced after 2.0 min reaction time. Particles were collected by centrifugation and washed once to remove any residual precursor and solvent.

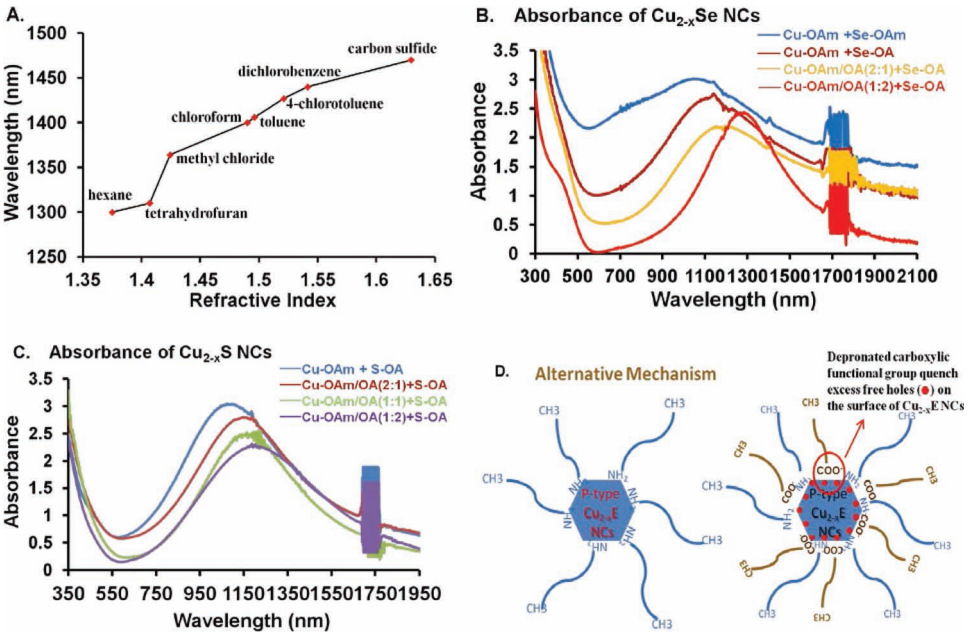

Figure 8. Dependence of LSPR frequency upon A) solvent refractive index for $Cu_{2-x}S$ NCs and B,C) ligand combination used in synthesis of B) $Cu_{2-x}Se$ NCs and C) $Cu_{2-x}S$ NCs. Panel (D) illustrates schematically the mechanism of carrier density reduction by coordination of deprotonated carboxyl groups to the NC surface.

of the NCs. Nonetheless, deprotonated oleic acid carries a negative charge, and coordination of deprotonated carboxyl groups to the surface may trap free holes and thereby reduce the effective free carrier concentration. The LSPR frequency red-shifts with decreasing carrier density. Changes in stoichiometry, size, and crystal structure upon addition of OA, as discussed above, can also contribute to the red-shift of the LSPR absorbance. This is particularly noticeable in Figure 8B, for particle prepared using only OAm (blue curve). These particles were a mixture of two phases with different stoichiometry (and therefore different free hole concentrations), and this is reflected in the broadened LSPR peak, which includes contributions from both phases. Interestingly, we found that there was no obvious change of LSPR in nanoparticles post-treated in pure OA at room temperature (Supporting Information Figure S8). However, when we aged the particles in pure OA at a somewhat elevated temperature (100 °C), red-shift of LSPR was observed (Supporting Information Figure S8). We thus conclude that there exists an activation barrier for OA to interact with the particle surface. Although the contributions of different mechanisms to the red-shift of the LSPR are not known quantitatively, this approach nonetheless allows the LSPR frequency to be tuned by choice of ligand, rather than by chemical oxidation or reduction of the NCs. This provides the important practical benefit of tuning the LSPR resonance during synthesis, producing colloidal dispersions of NCs with different LSPR frequency.

4. Conductivity and Optoelectronic Properties of $Cu_{2-x}Se$ and $Cu_{2-x}S$ NCs

The electrical conductivity of $Cu_{2-x}Se$ and $Cu_{2-x}S$ NCs thin films was studied in ITO-NC thin film-aluminum (Al) structures. **Figure 9**A schematically illustrates the device structure. Scanning electron microscopy (SEM, Figure 9B) of cross sections of $Cu_{2-x}S$ and $Cu_{2-x}Se$ NC thin films show film thicknesses of around 115 nm and 140 nm, respectively. Devices made from the as-deposited films of OA and OAm-capped particles showed insulating behavior, with currents of μA for the 0.0425 cm^2 device area and up to 1 V applied potential. To improve the charge mobility in NC thin films, short hydrocarbon ligands are preferred, to reduce interparticle distance and enhance interparticle coupling.

We selected three short bifunctional ligands, ethylenediamine (EDA), ethanedithiol (EDT) and mercaptopropionic acid (MPA) to treat the NC thin films. These displace the long-chain OA and OAm ligands present on the as-prepared particles. This chemical post-treatment led to an increase in electrical conductivity of the $Cu_{2-x}S$ and $Cu_{2-x}Se$ NCs thin films by about three orders of magnitude (**Figure 10**). We independently checked the conductivity of the treated $Cu_{2-x}S$ and $Cu_{2-x}Se$ NCs by depositing them on insulating glass substrates and measuring current parallel to the substrate surface (Supporting Information Figure S11). There also, current increased by three orders of magnitude upon EDT treatment. Currents of about 10^{-9} and 10^{-6} A were measured before and after treatment of these films (Supporting Information Figure S11). Consistency of this observation with the behavior of the stacked thin film structures provides confidence that the increased conductivity is not due to changes in film thickness or gaps in the film.

The $Cu_{2-x}S$ thin films treated with MPA showed higher conductance compared to those treated with EDT or EDA. This is consistent with the study by Jeong et al.[59] showing that treating lead sulfide QD-thin films with MPA produced higher mobility-lifetime product than treatment with other short ligands. They

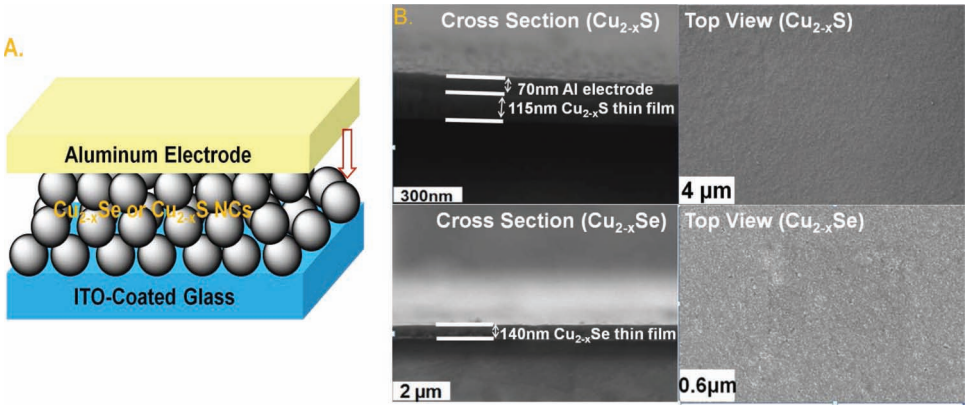

Figure 9. A) Schematically shows the device structure used for measuring film conductivity. B) SEM images of the cross section and top view of $Cu_{2-x}S$ and $Cu_{2-x}Se$ NCs thin film, respectively.

attributed that effect to the presence of two types of functional groups (thiol and carboxylate) in these ligands reducing defect densities. However, our experimental data showed that MPA-treated $Cu_{2-x}Se$ NCs thin films did not have higher conductivity than those treated with EDT, and EDA-treated films had even higher conductivity. This indicates that the underlying variable interactions between ligands and specific NCs result in different intraband trapping states, and that different ligands will therefore be optimal for different NCs.

The charge transport distance in the above measurements is the thickness of the NC film (measured by SEM as in Figure 9) and the device cross sectional area is 0.0425 cm^2. The untreated solution-processed $Cu_{2-x}S$ and $Cu_{2-x}Se$ NCs (OAm/OA capped) thin films exhibited conductance on the order of 10^{-8} S cm^{-1} and 10^{-9} S cm^{-1}, respectively. This is comparable to previously-reported dodecanethiol-capped Au NPs, which also showed conductance on the order of 10^{-9} S cm^{-1}.[13] The conductance of chemically-treated $Cu_{2-x}S$ and $Cu_{2-x}Se$ NC films was roughly three orders of magnitude higher, reaching 10^{-5} S cm^{-1} and 10^{-6} S cm^{-1}, respectively. The ligand exchange method used here is based on spin-coating the short ligands onto the NC film to replace the original long hydrocarbon ligands. This likely leads to incomplete ligand exchange. If samples were directly dipped into the short ligand solutions to achieve more complete ligand exchange, cracks in the film were observed, due to the reduced interparticle spacing, as previously observed by others.[14] With optimized post-treatment, the conductivity of solution-processed $Cu_{2-x}S$ and $Cu_{2-x}Se$ NC film could approach or even surpass that of Au and Ag NC films, given the higher conductivity exhibited by $Cu_{2-x}S$ and $Cu_{2-x}Se$ NC films before ligand exchange. This provides a promising possibility of using earth-abundant and cost-efficient semiconductor materials in place of noble metal-based NC thin films in solution-processed conductive films.

We also studied photoconductivity in $Cu_{2-x}S$ and $Cu_{2-x}Se$ NC thin films (Supporting Information Figure S12). The results did not show any dramatic increase in conductivity upon illumination, in contrast to previous investigations.[25] This may be partially accounted for by the fact that our NC films were much thinner than those in previous publications, resulting in weaker optical absorption. This becomes more obvious in a semiconductor with indirect band gap. Moreover, because of the high density of cationic vacancies in our $Cu_{2-x}S$ and $Cu_{2-x}Se$ NCs, the carrier concentration is already high without photoexcitation. The cationic vacancies may also increase the possibility of trapping photoexcited delocalized electrons. Nonetheless, the existence of a large concentration of free holes in the heavily self-doped NC film results in high conductivity providing a

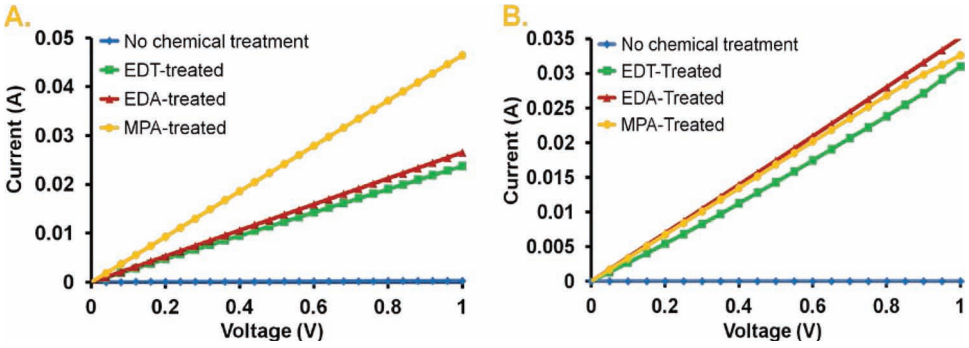

Figure 10. Current–voltage plots showing the conductivity of A) $Cu_{2-x}S$ film with no chemical treatment ($\sigma = 6.6 \times 10^{-8}$ S cm^{-1}), EDT-treated ($\sigma = 6.4 \times 10^{-6}$ S cm^{-1}), EDA-treated ($\sigma = 7.2 \times 10^{-6}$ S cm^{-1}), and MPA-treated ($\sigma = 1.3 \times 10^{-5}$ S cm^{-1}). B) $Cu_{2-x}Se$ film with no chemical treatment ($\sigma = 1.1 \times 10^{-9}$ S cm^{-1}), EDT-treated ($\sigma = 1.0 \times 10^{-5}$ S cm^{-1}), EDA-treated ($\sigma = 1.2 \times 10^{-5}$ S cm^{-1}), and MPA-treated ($\sigma = 1.1 \times 10^{-5}$ S cm^{-1}).

promising potential application in solution-processed field effect transistors.

5. Conclusion

In this work, we have demonstrated a facile method for controllable synthesis of highly self-doped $Cu_{2-x}S$ and $Cu_{2-x}Se$ NCs with significant localized surface plasmon resonance. The size and crystal phase of the nanocrystals was controlled by varying reaction time and coordinating solvent composition. The LSPR can be tuned over a relatively broad range by simply adjusting the concentration ratio of oleic acid and oleylamine used in synthesis. This provides a means of adjusting plasmonic absorption in self-doped semiconductor NCs by varying the ligands used in the synthesis, rather than by post-processing. Moreover, the investigation of $Cu_{2-x}Se$ and $Cu_{2-x}S$ NC thin films showed that they have high conductivity in ITO-NC-Al devices after replacing the long-hydrocarbon ligands used in synthesis with short-hydrocarbon ligands. These materials thus hold promise for application in next-generation solution-processed field effect transistors and other electronic devices.

6. Experimental Section

Chemicals: Copper (I) chloride (99.995%, Sigma Aldrich), oleylamine (technical grade 70%, Sigma Aldrich), oleylamine (approximate C_{18}-80–90%, Acros Organics), sulfur powder (90%, Sigma Aldrich), selenium powder (99.5%, Sigma Aldrich), and oleic acid (Fisher Scientific) were used as received, without further purification.

Methods: In general, the reactions described here were carried out using standard Schlenk-line techniques under nitrogen, without use of an inert-environment glove box. Post-processing was done in air.

Preparation of Organo-Copper Precursors: The copper precursor was prepared by dissolving 0.5 mmol copper (I) chloride into 10 mL oleylamine with heating at 220–230 °C until the solution was transparent. For investigating the effect of oleic acid, a mixture of oleylamine and oleic acid (at a concentration ratio OA/OAm ≤ 2:1) was used.

Preparation of Organo-Chalcogenide Precursors: S-OAm and S-OA precursors were prepared by mixing 1 mmol sulfur powder with 10 mL oleylamine or oleic acid and heating at 120 °C for 20–30 min. The Se-OAm or Se-OA precursor is synthesized the same way, but heated at 300–310 °C until a clear solution formed.

Synthesis of $Cu_{2-x}Se$ NCs in Pure Oleylamine: 5 mL Se-OAm solution was injected into 10 mL Cu(I)-OAm solution at 220 °C and held at this temperature. The reaction was stopped at representative time points, 1.5, 3, 5, and 8 min. $Cu_{2-x}Se$ nanodisks were prepared by injecting 5 mL Se-OAm precursor into 10 mL Cu(I)-OAm (Acros Organics) solution at 230 °C and holding the mixture at 220 °C for 3 min.

Synthesis of $Cu_{2-x}Se$ NCs in Oleylamine/Oleic Acid Mixtures: 5 ml Se-OA precursor was injected into 10 mL Cu(I)-OAm, Cu(I)-OAm/OA (2:1), or Cu(I)-OAm/OA(2:1) solution at 220 °C. The mixture was aged at this temperature for ≈5 min.

Size-Tunable Synthesis of $Cu_{2-x}S$ NCs: 2.8 nm $Cu_{2-x}S$ NCs were prepared by injecting 5 ml S-OAm (OAm is from Acros Organics) into 10 mL Cu(I)-OAm solution at 140 °C. The temperature was held at 132 °C for about 2 min. 6.8 nm $Cu_{2-x}S$ NCs were prepared by injecting 5 mL S-OAm (OAm is from Sigma Aldrich) into 10 mL Cu(I)-OAm solution at 115 °C. The temperature was held at 100 °C for about 3 min. 8.8 nm $Cu_{2-x}S$ NCs were prepared by injecting 5 mL S-OAm (OAm is from Sigma Aldrich) into 10 mL Cu(I)-OAm solution at 125 °C. The temperature was held at 107 °C for about 1.5 min. 11.5 nm $Cu_{2-x}S$ NCs were prepared by injecting 5 mL S-OAm (OAm is from Sigma Aldrich) into 10 mL Cu(I)-OAm solution at 125 °C. The temperature was held at 107 °C for about 3 min. 13.5 nm $Cu_{2-x}S$ NCs were prepared by injecting 5 mL S-OA into 10 mL Cu(I)-OAm solution at 140 °C. The temperature was held at 133 °C for about 2 min.

Purification: Ethanol was added to the reaction solution at 60–80 °C followed by centrifuging at 8000 rpm for about 1.5 min. $Cu_{2-x}S$ and $Cu_{2-x}Se$ NCs can be well dispersed in non-polar organic solvents including chloroform, hexane and toluene. This procedure was repeated twice to remove residual surfactants.

Transmission Electron Microscopy: The size and morphology of NCs were determined by transmission electron microscopy (TEM) using a JEOL JEM-2010 microscope at a working voltage of 200 kV. Selected area electron diffraction (SAED) patterns were obtained in the same instrument.

UV-Vis-NIR Spectroscopy: Optical absorbance of colloidal $Cu_{2-x}S$ and $Cu_{2-x}Se$ NCs was measured using a Shimadzu 3600 UV–visible-NIR scanning spectrophotometer.

X-Ray Diffraction: Powder XRD (Bruker Ultima IV with Cu Kα X-ray) was employed to characterize the crystal structure of the $Cu_{2-x}S$ and $Cu_{2-x}Se$ NCs. Samples were prepared by drop-casting high-concentration colloidal $Cu_{2-x}S$ and $Cu_{2-x}Se$ NC dispersions onto glass.

Scanning Electron Microscopy: Images of NC thin films were obtained by scanning electron microscopy (SEM) using a Carl Zeiss SEM ultra 40 XB under a EHT voltage of 5 kV. Samples were prepared by layer-by-layer spin coating onto ITO-coated glass.

Energy Dispersive X-Ray Spectrometry: Quantitative elemental analysis of NCs was obtained using Oxford Instruments X-Max 20 mm^2 energy dispersive X-ray spectrometer (EDS) detector.

Thermogravimetric Analysis: A NETSCH TGA 209 F1 thermal analyzer was used to acquire TGA data. Samples were heated at a rate of 10 °C/min under slow nitrogen flow.

Fourier Transform Infrared Spectroscopy (FTIR): A Bruker Vertex 70 FTIR spectrometer was used for FTIR characterization. Samples were prepared by drop-casting concentrated $Cu_{2-x}Se$ and $Cu_{2-x}S$ NCs on the ZnSe crystal substrate.

Investigation of Conductivity and Photoconductivity of NC Thin Film: Devices with standard vertical structure (ITO-NC-Al) were employed to examine electronic and optoelectronic properties of $Cu_{2-x}Se$ and $Cu_{2-x}S$ NC thin films. Conductivity and photoconductivity of devices were measured using a Labview-controlled voltage/source meter (Keithley 2400) in the dark and under AM 1.5G condition (100 mW/cm^2), respectively.

The ITO-NC-Al structures were fabricated as follows. First, an ITO-coated glass substrate (1.25 cm × 1.25 cm) was cleaned using acetone, methanol and de-ionized water. Then $Cu_{2-x}Se$ or $Cu_{2-x}S$ NCs were spin cast on the ITO-coated glass substrates at 1000 rpm for 40 s. Then the substrate was heated at 75–80 °C for 10 min under nitrogen protection to densify the NC film. 1,2-ethanedithiol (EDT, 0.01 M) solution in acetonitrile (AcCN), 3-mercaptopropionic acid in ethanol (10% by volume) and ethylenediamine solution in AcCN (60 mg/mL) were prepared for further chemical treatment of NC films. Then, EDT, MPA or EDA solution was deposited onto the nanocrystal film and spin-coated at 2500 rpm for 15 s to replace the oleylamine/oleic acid ligands. Then sample was rinsed with pure AcCN and hexane to remove the exchanged oleic acid and any residual EDT, MPA, or EDA. After that, the sample was heated at 80 °C for 10 min under nitrogen protection. Finally, a 70 nm Al layer was deposited using an electron beam evaporator at a deposition rate of 0.6 Å/s under 5×10^{-7} Torr with active area 4.25 mm^2.

Supporting Information

Supporting Information is available from the Wiley Online Library or from the author.

Received: July 24, 2012
Revised: September 7, 2012
Published online: October 15, 2012

[1] C. B. Murray, D. J. Norris, M. G. Bawendi, *J. Am. Chem. Soc.* **1993**, *115*, 8706–8715.
[2] A. P. Alivisatos, *Science* **1996**, *271*, 933–937.
[3] X. G. Peng, L. Manna, W. D. Yang, J. Wickham, E. Scher, A. Kadavanich, A. P. Alivisatos, *Nature* **2000**, *404*, 59–61.
[4] Z. A. Peng, X. G. Peng, *J. Am. Chem. Soc.* **2001**, *123*, 183–184.
[5] W. U. Huynh, J. J. Dittmer, A. P. Alivisatos, *Science* **2002**, *295*, 2425–2427.
[6] I. Gur, N. A. Fromer, M. L. Geier, A. P. Alivisatos, *Science* **2005**, *310*, 462–465.
[7] K. W. Johnston, A. G. Pattantyus-Abraham, J. P. Clifford, S. H. Myrskog, D. D. MacNeil, L. Levina, E. H. Sargent, *Appl. Phys. Lett.* **2008**, *92*.
[8] J. Tang, K. W. Kemp, S. Hoogland, K. S. Jeong, H. Liu, L. Levina, M. Furukawa, X. H. Wang, R. Debnath, D. K. Cha, K. W. Chou, A. Fischer, A. Amassian, J. B. Asbury, E. H. Sargent, *Nat. Mater.* **2011**, *10*, 765–771.
[9] Y. Wu, C. Wadia, W. L. Ma, B. Sadtler, A. P. Alivisatos, *Nano Lett.* **2008**, *8*, 2551–2555.
[10] P. V. Kamat, *J. Phys. Chem. C* **2008**, *112*, 18737–18753.
[11] J. H. Bang, P. V. Kamat, *ACS Nano* **2009**, *3*, 1467–1476.
[12] W. L. Ma, S. L. Swisher, T. Ewers, J. Engel, V. E. Ferry, H. A. Atwater, A. P. Alivisatos, *ACS Nano* **2011**, *5*, 8140–8147.
[13] M. V. Kovalenko, M. Scheele, D. V. Talapin, *Science* **2009**, *324*, 1417–1420.
[14] J. H. Choi, A. T. Fafarman, S. J. Oh, D. K. Ko, D. K. Kim, B. T. Diroll, S. Muramoto, J. G. Gillen, C. B. Murray, C. R. Kagan, *Nano Lett.* **2012**, *12*, 2631–2638.
[15] D. V. Talapin, C. B. Murray, *Science* **2005**, *310*, 86–89.
[16] Z. C. Holman, C. Y. Liu, U. R. Kortshagen, *Nano Lett.* **2010**, *10*, 2661–2666.
[17] G. Konstantatos, I. Howard, A. Fischer, S. Hoogland, J. Clifford, E. Klem, L. Levina, E. H. Sargent, *Nature* **2006**, *442*, 180–183.
[18] E. H. Sargent, *Adv. Mater.* **2008**, *20*, 3958–3964.
[19] D. V. Talapin, J. S. Lee, M. V. Kovalenko, E. V. Shevchenko, *Chem. Rev.* **2010**, *110*, 389–458.
[20] M. B. Sigman, A. Ghezelbash, T. Hanrath, A. E. Saunders, F. Lee, B. A. Korgel, *J. Am. Chem. Soc.* **2003**, *125*, 16050–16057.
[21] W. P. Lim, C. T. Wong, S. L. Ang, H. Y. Low, W. S. Chin, *Chem. Mater.* **2006**, *18*, 6170–6177.
[22] S. H. Choi, K. An, E. G. Kim, J. H. Yu, J. H. Kim, T. Hyeon, *Adv. Funct. Mater.* **2009**, *19*, 1645–1649.
[23] Y. Wang, Y. X. Hu, Q. Zhang, J. P. Ge, Z. D. Lu, Y. B. Hou, Y. D. Yin, *Inorg. Chem.* **2010**, *49*, 6601–6608.
[24] S. C. Riha, D. C. Johnson, A. L. Prieto, *J. Am. Chem. Soc.* **2011**, *133*, 1383–1390.
[25] J. Choi, N. Kang, H. Y. Yang, H. J. Kim, S. U. Son, *Chem. Mater.* **2010**, *22*, 3586–3588.
[26] R. Yu, T. Ren, K. J. Sun, Z. C. Feng, G. N. Li, C. Li, *J. Phys. Chem. C* **2009**, *113*, 10833–10837.
[27] A. Ghezelbash, B. A. Korgel, *Langmuir* **2005**, *21*, 9451–9456.
[28] L. Chen, Y. B. Chen, L. M. Wu, *J. Am. Chem. Soc.* **2004**, *126*, 16334–16335.
[29] C. R. Lubeck, T. Y. J. Han, A. E. Gash, J. H. Satcher, F. M. Doyle, *Adv. Mater.* **2006**, *18*, 781–784.
[30] J. Xu, C. S. Lee, Y. B. Tang, X. Chen, Z. H. Chen, W. J. Zhang, S. T. Lee, W. X. Zhang, Z. H. Yang, *ACS Nano* **2010**, *4*, 1845–1850.
[31] M. Lotfipour, T. Machani, D. P. Rossi, K. E. Plass, *Chem. Mater.* **2011**, *23*, 3032–3038.
[32] M. G. Panthani, V. Akhavan, B. Goodfellow, J. P. Schmidtke, L. Dunn, A. Dodabalapur, P. F. Barbara, B. A. Korgel, *J. Am. Chem. Soc.* **2008**, *130*, 16770–16777.
[33] Q. Guo, G. M. Ford, H. W. Hillhouse, R. Agrawal, *Nano Lett.* **2009**, *9*, 3060–3065.
[34] Q. J. Guo, H. W. Hillhouse, R. Agrawal, *J. Am. Chem. Soc.* **2009**, *131*, 11672–11673.
[35] B. Koo, R. N. Patel, B. A. Korgel, *J. Am. Chem. Soc.* **2009**, *131*, 3134–3135.
[36] C. Steinhagen, M. G. Panthani, V. Akhavan, B. Goodfellow, B. Koo, B. A. Korgel, *J. Am. Chem. Soc.* **2009**, *131*, 12554–12555.
[37] A. Shavel, J. Arbiol, A. Cabot, *J. Am. Chem. Soc.* **2010**, *132*, 4514–4515.
[38] T. Kameyama, T. Osaki, K. Okazaki, T. Shibayama, A. Kudo, S. Kuwabata, T. Torimoto, *J. Mater. Chem.* **2010**, *20*, 5319–5324.
[39] N. Z. Bao, X. M. Qiu, Y. H. A. Wang, Z. Y. Zhou, X. H. Lu, C. A. Grimes, A. Gupta, *Chem. Commun.* **2011**, *47*, 9441–9443.
[40] H. Z. Zhong, Z. B. Wang, E. Bovero, Z. H. Lu, F. C. J. M. van Veggel, G. D. Scholes, *J. Phys. Chem. C* **2011**, *115*, 12396–12402.
[41] S. H. Choi, E. G. Kim, T. Hyeon, *J. Am. Chem. Soc.* **2006**, *128*, 2520–2521.
[42] M. Kar, R. Agrawal, H. W. Hillhouse, *J. Am. Chem. Soc.* **2011**, *133*, 17239–17247.
[43] Y. X. Zhao, H. C. Pan, Y. B. Lou, X. F. Qiu, J. J. Zhu, C. Burda, *J. Am. Chem. Soc.* **2009**, *131*, 4253–4261.
[44] J. M. Luther, P. K. Jain, T. Ewers, A. P. Alivisatos, *Nat. Mater.* **2011**, *10*, 361–366.
[45] D. Dorfs, T. Hartling, K. Miszta, N. C. Bigall, M. R. Kim, A. Genovese, A. Falqui, M. Povia, L. Manna, *J. Am. Chem. Soc.* **2011**, *133*, 11175–11180.
[46] F. Scotognella, G. Della Valle, A. R. S. Kandada, D. Dorfs, M. Zavelani-Rossi, M. Conforti, K. Miszta, A. Comin, K. Korobcheyskaya, G. Lanzani, L. Manna, F. Tassone, *Nano Lett.* **2011**, *11*, 4711–4717.
[47] C. M. Hessel, V. P. Pattani, M. Rasch, M. G. Panthani, B. Koo, J. W. Tunnell, B. A. Korgel, *Nano Lett.* **2011**, *11*, 2560–2566.
[48] Q. W. Tian, F. R. Jiang, R. J. Zou, Q. Liu, Z. G. Chen, M. F. Zhu, S. P. Yang, J. L. Wang, J. H. Wang, J. Q. Hu, *ACS Nano* **2011**, *5*, 9761–9771.
[49] S. W. Hsu, K. On, A. R. Tao, *J. Am. Chem. Soc.* **2011**, *133*, 19072–19075.
[50] H. L. Li, Y. C. Zhu, S. Avivi, O. Palchik, J. P. Xiong, Y. Koltypin, V. Palchik, A. Gedanken, *J. Mater. Chem.* **2002**, *12*, 3723–3727.
[51] S. Deka, A. Genovese, Y. Zhang, K. Miszta, G. Bertoni, R. Krahne, C. Giannini, L. Manna, *J. Am. Chem. Soc.* **2010**, *132*, 8912–8914.
[52] I. Kriegel, J. Rodriguez-Fernandez, E. Da Como, A. A. Lutich, J. M. Szeifert, J. Feldmann, *Chem. Mater.* **2011**, *23*, 1830–1834.
[53] Y. Liu, Q. F. Dong, H. T. Wei, Y. Ning, H. Z. Sun, W. J. Tian, H. Zhang, B. Yang, *J. Phys. Chem. C* **2011**, *115*, 9909–9916.
[54] H. Zhang, Y. Q. Zhang, J. X. Yu, D. R. Yang, *J. Phys. Chem. C* **2008**, *112*, 13390–13394.
[55] L. Lutterotti, *Nucl. Instrum. Meth. B* **2010**, *268*, 334–340.
[56] W. J. Baumgardner, J. J. Choi, Y. F. Lim, T. Hanrath, *J. Am. Chem. Soc.* **2010**, *132*, 9519–9521.
[57] J. Thessing, J. H. Qian, H. Y. Chen, N. Pradhan, X. G. Peng, *J. Am. Chem. Soc.* **2007**, *129*, 2736–2737.
[58] I. Kriegel, C. Y. Jiang, J. Rodriguez-Fernandez, R. D. Schaller, D. V. Talapin, E. da Como, J. Feldmann, *J. Am. Chem. Soc.* **2012**, *134*, 1583–1590.
[59] K. S. Jeong, J. Tang, H. Liu, J. Kim, A. W. Schaefer, K. Kemp, L. Levina, X. H. Wang, S. Hoogland, R. Debnath, L. Brzozowski, E. H. Sargent, J. B. Asbury, *ACS Nano* **2012**, *6*, 89–99.